Newcastle University

ePrints

Ma Z, Bao H, Roskilly AP. Performance analysis of ultralow grade waste heat upgrade using absorption heat transfer. *Applied Thermal Engineering* 2016, DOI: 10.1016/j.applthermaleng.2016.02.002

Copyright:

© 2016 Published by Elsevier Ltd. under a Creative Commons license

DOI link to article:

http://dx.doi.org/10.1016/j.applthermaleng.2016.02.002

Date deposited:

23/03/2016

This work is licensed under a Creative Commons Attribution 4.0 International License

Newcastle University ePrints - eprint.ncl.ac.uk

Applied Thermal Engineering ■■ (2016) ■■–■■

Contents lists available at ScienceDirect

Applied Thermal Engineering

journal homepage: www.elsevier.com/locate/apthermeng

Research Paper

Performance analysis of ultralow grade waste heat upgrade using absorption heat transformer

Zhiwei Ma *, Huashan Bao, Anthony Paul Roskilly

Sir Joseph Swan Centre for Energy Research, Newcastle University, Newcastle upon Tyne NE1 7RU, United Kingdom

HIGHLIGHTS

- Upgrade ultralow grade waste heat at 40~60 °C using absorption heat transformers.
- The recirculation flow ratio was found to be the most direct and crucial factor.
- The single stage transformer had medium temperature lift with a medium efficiency.
- The double stage transformer can achieve almost doubled temperature lift.
- The double effect transformer was not suitable for ultralow grade waste heat.

ARTICLE INFO

Article history:
Received 21 October 2015
Accepted 1 February 2016
Available online

Keywords:
Absorption heat transformer
Ultralow grade waste heat
Temperature lift
Coefficient of performance
Lithium bromide solution

ABSTRACT

The present paper aimed at exploring absorption heat transformer (AHT) to upgrade ultralow grade waste heat in the temperature range of 40–60 °C. The performance of AHTs with different configurations, including single stage, double stage and double effect, were numerically analysed and compared in terms of temperature lift, coefficient of performance (*COP*) and exergy coefficient of performance (*COPe*). The most influential and crucial factor for the studied AHTs is the recirculation flow ratio (*FR*), the increase of which results in an increasing temperature lift but gradually declining *COP*. The *COPe* can achieve its maximum value with a certain *FR*, and such a state can be considered as the optimal working condition. Within the studied waste heat temperature range, the optimal *FR* in single stage AHT is in the range of 10–12, at which the system can deliver 17.1~34.7 °C temperature lift with *COP* at 0.471~0.475. The best configuration amid the studied four different double stage AHTs has a temperature lifting capacity of 31.8~68.6 °C with a *COP* around 0.30. The double effect AHT compromises its temperature lifting capacity for the highest *COP* among all the AHTs studied, which can reach about 0.65 though necessitates relatively higher waste heat temperature and higher strong solution concentration to drive the cycle; the double effect AHT is not recommended for the upgrading of ultralow grade waste heat.

© 2016 Published by Elsevier Ltd.

1. Introduction

Energy demand in industry sectors accounts for around 17% of the total energy consumption in the UK [1], and the worse thing is that the average industrial thermal waste via radiation, exhausted gas or air, cooling fluids and so on is about one sixth of this total energy demand [2]. In fact, the wasted heat still contains large amount of energy and exergy that can be reused to deliver heating, cooling or work through suitable heat recovery technologies. There has been a great number of promising and interesting technologies emerging to realise the recovery of waste heat prevailingly around 70~250 °C, like power generation via organic Rankine cycle [3] and Kalina cycle [4], refrigeration by absorption [5] and adsorption [6] technologies, and district heating [7], etc. More efforts are encouraged to address the significant though more challenging and less explored cases, the recovery and utilisation of the ultralow grade waste heat, which in the temperature range between 40 and 60 °C is way more ubiquitous and could account for about 30% of the total industrial waste heat [8]. With rational heat recovery and effective heat transformer technologies, these waste heat could play an important role on energy saving and sustainable development.

Absorption heat transformer (AHT), operating in the reverse way of absorption refrigeration, can economically upgrade low grade waste heat into useful heat at a higher temperature with only little electrical energy input for pumping work [9,10]. It is reported that a single stage AHT (SAHT) can recover approximately 50% of waste heat with a temperature lift of about 50 °C in principle [10], after which the useful energy can be reused in industrial processes.

The SAHT performance of using LiBr–H_2O solution and H_2O–NH_3 solution, as the two most commonly used working solutions,

* Corresponding author. Tel.: +44 001912464849; fax: +44 001912226920.
E-mail address: zhiwei.ma@newcastle.ac.uk (Z. Ma).

http://dx.doi.org/10.1016/j.applthermaleng.2016.02.002
1359-4311/© 2016 Published by Elsevier Ltd.

Please cite this article in press as: Zhiwei Ma, Huashan Bao, Anthony Paul Roskilly, Performance analysis of ultralow grade waste heat upgrade using absorption heat transformer, Applied Thermal Engineering (2016), doi: 10.1016/j.applthermaleng.2016.02.002

were compared by Kurem and Horuz [11]. The comparison showed that LiBr–H_2O solution out-performed its rival, though the temperature lift was limited by the crystallisation issue. To further enhance the performance of LiBr–H_2O based SAHT, Rivera et al. [12] used a commercial compound named Carrol, which was a mixture of LiBr and ethylene glycol in the mass ratio of 1:4.5 with water as the working solution. Carrol has higher solubility in water than LiBr does, which makes it a favourable alternative working solution for AHT. Rivera and Cerezo [13] and Rivera et al. [14] added 400 ppm 2-ethyl-1-hexanol into LiBr–H_2O solution as a heat and mass transfer enhancer so that the upgraded temperature and the coefficient of performance (*COP*) was improved by 5 °C and 40%, respectively. Barragan et al. [15–18] conducted a series of experimental studies using LiCl–H_2O, $CaCl_2$–H_2O, $MgCl_2$–H_2O and also ternary solutions of LiCl–$ZnCl_2$–H_2O and $CaCl_2$–$ZnCl_2$–H_2O in SAHT. The test results showed lower temperature lift by using $CaCl_2$–H_2O or $MgCl_2$–H_2O solution than using LiCl–H_2O solution due to the lower solubility of $CaCl_2$ and $MgCl_2$ in water. It was also found that the addition of $ZnCl_2$ in the ternary solution could reduce the solution viscosity and eliminate the solution crystallisation. Yin et al. [19] compared the performance of using LiBr–H_2O, TFE (2, 2, 2-trifluoroethanol)–NMP (*N*-methyl-2-pyrrolidone), TFE–E181 (dimethylether tetraethylene glycol) and TFE–PYR (2-pyrrolidone) as working solution in SAHT. It concluded that the LiBr–H_2O based SAHT performed superiorly when the output temperature was below 150 °C, while the other three solutions were more stable at higher temperature, e.g. up to 200 °C. The authors therefore suggested a double stage system using LiBr–H_2O loop in the lower temperature cycle while using one of the other three in the higher temperature cycle to achieve higher temperature lift.

Alternatively, Horuz and Kurt [20] and Parham et al. [21] tried different configurations to improve the performance of SAHT. Three more configurations other than the conventional configuration (named as SAHT-1 in present paper) were introduced and evaluated, including SAHT-2 in which the water carrying waste heat transferred the heat to the evaporator prior to the generator; SAHT-3 in which it had an additional absorber heat exchanger on the basis of SAHT-2; and SAHT-4 in which it was based on SAHT-3 and mounted with another refrigerant heat exchanger at the inlet of evaporator. These three new configurations reduced the crystallisation risk of using LiBr–H_2O as working solution. Both studies concluded the *COP* value in the order of SAHT-4 > SAHT-3 > SAHT-1 > SAHT-2, and the highest *COP* value was about 13–14% higher than the lowest one.

Double stage AHT (DAHT) can be applied if larger temperature lift is expected, which was reported to be capable of achieving about 80 °C temperature lift with a *COP* of 0.35 [10]. Several types of DAHT cycles have been proposed to explore the preferable configuration for optimal efficiency and effective heat transformation. The typical straightforward approach to implement DAHT (named as DAHT-1 in the present paper) is to couple two sets of SAHT units through the heat exchanging between the absorber in the low temperature loop and the evaporator in the high temperature loop [22–26]. Romero et al. [24] experimentally demonstrated that the DAHT-1 could transform the heat from 80 °C to 152 °C with efficiency higher than 30%. Ji and Ishida [26] studied a DAHT-1 system where both the absorber and the generator were peculiarly designed with two or more interior compartments, and found that the temperature lift was improved by around 10.7 °C and the exergy efficiency was elevated from 48.14% to 54.95% due to the usage of these compartments.

Rivera et al. [23] proposed a different DAHT cycle (named as DAHT-2) and claimed it to be technically simpler and competent comparing to DAHT-1. DAHT-2 utilises a portion of the weak solution from the high temperature absorber as the strong solution for the low temperature absorber. Martinez and Rivera [27] conducted theoretical energy and exergy analysis on DAHT-2, and concluded that the system could generate a 74 °C temperature lift. Furthermore, they suggested that the generator was responsible for the highest thermodynamic irreversibility, which was about 40% of the total exergy destruction. Reyes et al. [28] modelled the DAHT-2 system using $CaCl_2$–H_2O and LiCl–H_2O, which could achieve typical temperature lifts around 35~40 °C.

Based on DAHT-2, Zhao et al. [29] developed a new DAHT (named as DAHT-3) that splits the strong solution from the generator into two streams – one heading for high temperature absorber and the other one for low temperature absorber. This new arrangement introduced 5~10 °C increase in temperature lift contrasted with DAHT-2, while the *COP* marginally dropped by 0.01. Similar analytical conclusions were also obtained by Horuz and Kurt [30].

Mostofizadeh and Kulick [31] reported another different configuration of DAHT (named as DAHT-4), which had all the weak solution from high temperature absorber received by the low temperature absorber as the second stage of absorption. Subsequently, the weaker solution exiting the low temperature absorber ended up in the generator. Zhao et al. [32] reported that the DAHT-4 had the largest *COP* especially when the heat output temperature, namely the absorption temperature, was required higher, as the maximum *COP* value could reach 0.32 with the temperature lift between 60 and 100 °C.

Double effect absorption heat transformer (DeAHT) was developed to satisfy the desire of higher system efficiency, while the heat upgrading level is inevitably compromised. Zhao et al. [33] investigated the DeAHT system using TFE–E181 and LiBr–H_2O as working solutions, and the analytical results showed a 30 °C temperature lift could be achieved with waste heat temperature at 70 °C; the corresponding *COP* value was as high as 0.58 and 0.64, respectively for the studied two working solutions. Gomri [34] comparatively applied the SAHT and DeAHT to the seawater desalination with heat input at the temperature of 74~96 °C and 87~96 °C, and obtained 103~158 °C and 103~123 °C upgraded heat, respectively.

Though AHTs have been widely investigated and reported, to the best of the authors' knowledge, there has been neither endeavour in recovering and upgrading ultralow grade waste heat in the temperature range between 40 and 60 °C nor the comprehensive comparative study on various AHT systems including all aforementioned cycles. Therefore, this work carried out analytical study on six different AHTs using LiBr–H_2O with primary interest in heat transformation of the ultralow grade heat from 40 to 60 °C.

2. Working principles of AHTs and analysis methods

The schematics of each type of AHT systems studied in this work are depicted in this section associated with the details of the predefined temperature, pressure and concentration in P–T–x diagram. All the plotted properties of LiBr–H_2O solution in vapour–liquid equilibrium states were calculated by the formulas provided in Pátek and Klomfar's work [35].

The following assumptions were predefined to simplify the calculation:

1. The analysis was carried out at steady-state conditions;
2. The solutions at the outlets of generator and absorber were at saturated state;
3. The refrigerants, water, at the outlets of condenser and evaporator were at saturated state;
4. The pumping work was neglected; therefore, the temperature and enthalpy of the fluid before and after the pump remained unchanged;
5. Throttling did not change the enthalpy of the fluid;
6. No heat loss from any well-insulated components.

Please cite this article in press as: Zhiwei Ma, Huashan Bao, Anthony Paul Roskilly, Performance analysis of ultralow grade waste heat upgrade using absorption heat transformer, Applied Thermal Engineering (2016), doi: 10.1016/j.applthermaleng.2016.02.002

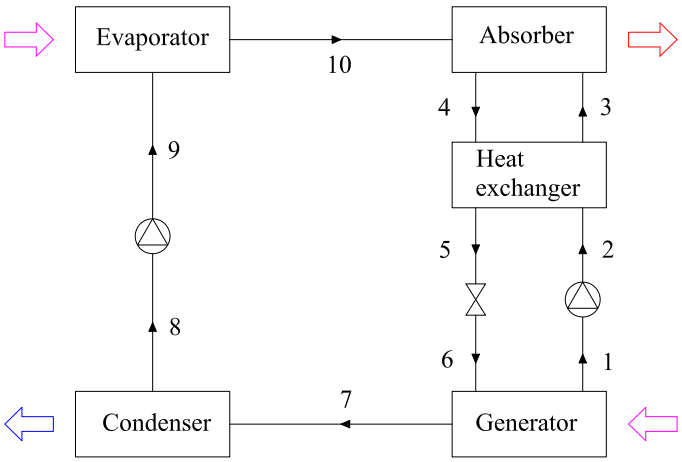

(a)

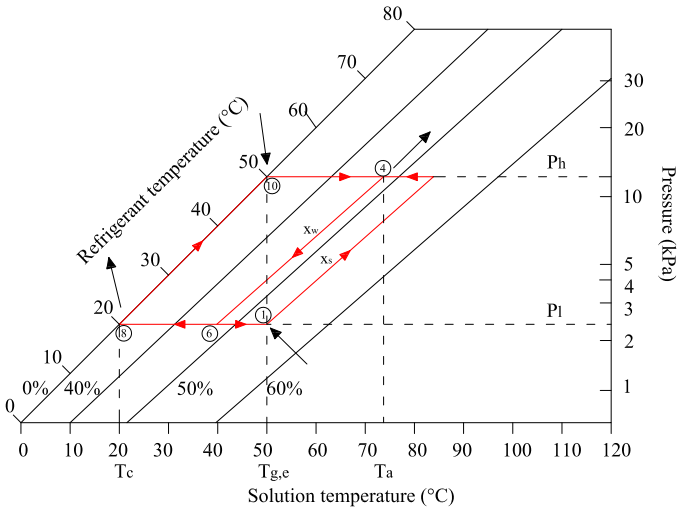

(b)

Fig. 1. SAHT. (a) Schematic diagram; (b) P–T–x diagram.

2.1. SAHT

The schematic diagram of SAHT (SAHT-1) in Fig. 1(a) consists of a generator, a condenser, an evaporator, an absorber and a heat exchanger while the first two components are at low pressure level and the last three are at high pressure level. The thermodynamic cycle in P–T–x diagram is exemplified with 50 °C waste heat and 20 °C condensation temperature as shown in Fig. 1(b).

The waste heat is used to separate the binary mixture in the generator by partially evaporating the refrigerant, i.e. the water, so that the solution within the generator becomes richer in LiBr and heads for the absorber. On its way to the absorber, the strong solution is firstly pumped to higher pressure (stream 1–2) and subsequently pre-heated (stream 2–3) by the return weak solution coming down from the absorber (stream 4–5) which is at higher temperature. The desorbed refrigerant vapour (point 7) from the generator is liquefied in the condenser (stream 7–8) and pumped up to higher pressure level (stream 8–9) before entering into the evaporator. The evaporator is supplied with waste heat again to generate higher pressure refrigerant vapour (point 10) which afterwards is thoroughly absorbed by the strong solution in the absorber so that the exothermic absorption process releases heat at a temperature higher than the heat source temperature due to the higher pressure. The weak solution from the absorber should be throttled (stream 5–6) after heat recovery to charge the low pressure generator.

According to the predefined assumption, the refrigerant at point 8 and point 10 are saturated liquid and saturated vapour, respectively, so that their enthalpies (h_8 and h_{10}) can be determined solely by the condensation temperature (T_c) and evaporation temperature ($T_{g,e}$). The refrigerant enthalpy remains unchanged through the pump, i.e. h_9 is equal to h_8. The enthalpy value of refrigerant at point 7 (h_7) can be calculated by considering both the refrigerant pressure and temperature equal to the generator pressure and temperature, respectively. The waste heat input to the evaporator (Q_e) can be calculated by Eq. (1).

$$Q_e = \dot{m}_r (h_{10} - h_9) \tag{1}$$

where $\dot{m}_r$ is the mass flow rate of refrigerant.

Considering the saturated states of refrigerant at point 8 and point 10, the condensing temperature T_c can be used to determine the low working pressure (P_l) across the generator and the condenser, while the waste heat temperature imposing on the evaporator determines the high working pressure (P_h) that dominates the evaporator and the absorber. Since the solution is saturated at point 1, the strong solution concentration (x_s) is then considered as the saturated solution concentration under the conditions of pressure P_l and temperature $T_{g,e}$. The recirculation flow ratio (FR) as defined in Eq. (2) should be given to determine the weak solution concentration (x_w), the flow rates of the weak solution ($\dot{m}_w$) and strong solution ($\dot{m}_s$) while combining with mass balance equations, Eqs. (3) and (4), the already attained x_s and given $\dot{m}_r$.

$$FR = \frac{\text{mass flow rate of solution leaving generator}}{\text{mass flow rate of vapour leaving generator}} = \frac{\dot{m}_s}{\dot{m}_r} \tag{2}$$

$$\dot{m}_s x_s = \dot{m}_w x_w \tag{3}$$

$$\dot{m}_r + \dot{m}_s = \dot{m}_w \tag{4}$$

Thereafter, the upgraded temperature in the absorber (T_a) can be conveniently determined as it is at intersection point of high pressure (P_h) and the weak solution concentration (x_w) as shown in Fig. 1(b).

The enthalpy of the saturated strong solution at the outlet of the generator (h_1) can be determined by its temperature ($T_1 = T_{g,e}$) and the low pressure (P_l); by the same way, the outlet weak solution enthalpy (h_4) from the absorber can be determined by its temperature ($T_4 = T_a$) and the high pressure (P_h). For the heat exchanger, the inlet thermal states of the counter-flow solution streams become known because the temperature and enthalpy values at point 2 equal to those of point 1 according to the assumption. With a given performance parameter UA, i.e. the multiplicative product of heat transfer coefficient and heat transfer area of the heat exchanger, the outlet temperature (T_3 and T_5) and enthalpy (h_3 and h_5) of the weak and strong solutions, those that have heat exchanging can be iteratively determined through energy equations, Eq. (5) and Eq. (6), the logarithmic temperature difference ΔT_{LMTD} in Eq. (7) and the correlation of solution enthalpy with temperature and concentration.

$$Q_{HE} = \Delta T_{LMTD} \cdot UA \tag{5}$$

$$Q_{HE} = \dot{m}_s h_3 - \dot{m}_s h_2 = \dot{m}_w h_4 - \dot{m}_w h_5 \tag{6}$$

$$\Delta T_{LMTD} = \frac{T_4 - T_3 - (T_5 - T_2)}{\ln\left(\frac{T_4 - T_3}{T_5 - T_2}\right)} \tag{7}$$

Please cite this article in press as: Zhiwei Ma, Huashan Bao, Anthony Paul Roskilly, Performance analysis of ultralow grade waste heat upgrade using absorption heat transformer, Applied Thermal Engineering (2016), doi: 10.1016/j.applthermaleng.2016.02.002

Then, the enthalpy of the inlet weak solution (h_6) to the generator is known as the same with that of point 5 (h_5). With all known variables on the right-hand side of energy balance equations (Eq. (8) and Eq. (9)), the heat input to the generator (Q_g) and the heat generated in the absorber (Q_a) can be obtained.

$$Q_g = \dot{m}_s h_1 + \dot{m}_r h_7 - \dot{m}_w h_6 \tag{8}$$

$$Q_a = \dot{m}_s h_3 + \dot{m}_r h_{10} - \dot{m}_w h_4 \tag{9}$$

Finally, the coefficient of performance (*COP*) and exergy *COP* (*COPe*) of the SAHT cycle can be calculated by Eq. (10) and Eq. (11), respectively.

$$COP = \frac{Q_a}{Q_e + Q_g} \tag{10}$$

$$COPe = \frac{Q_a\left(1 - \frac{T_c}{T_a}\right)}{(Q_e + Q_g)\left(1 - \frac{T_c}{T_{g,e}}\right)} \tag{11}$$

2.2. DAHT-1

Based on the design of SAHT, one more heat exchanger and one more absorber are added in to form the DAHT-1 as illustrated in Fig. 2(a), where three pressure levels are established to gradually elevate the temperature of the waste heat. The two absorbers are at different pressures, as tagged low pressure absorber (L-Absorber) and high pressure absorber (H-Absorber), respectively. DAHT-1 basically integrates two single effect cycles by splitting refrigerant stream from the condenser into two sub-streams, one of which is pumped to the evaporator (stream 14-15-16-17) before arriving in the L-Absorber while the other sub-stream is directly heading to the H-Absorber (stream 14-18-19-20) through a relatively more powerful pumping. Likewise, the strong solution from the generator is also split, one part of which is less pumped, heated and received by the L-Absorber (stream 7-8-9), while the rest is strongly pumped, heated and received by the H-Absorber (stream 1-2-3). The first sub-stream of the refrigerant evaporates and mixes with partial strong solution in the L-Absorber whereby the absorption heat is released at a temperature higher than the waste heat source; the second sub-stream refrigerant boils by this upgraded heat in the L-Absorber so that the generated vapour is at an even higher pressure, which subsequently thoroughly mixes with the strong solution in the H-Absorber to achieve further heat upgrading.

The low pressure, P_l, and medium pressure, P_m, can be firstly determined by the condensation temperature and waste heat temperature as shown in Fig. 2(b). Four different solution concentrations are involved in this cycle, including strong solution concentrations at different pressure levels, x_{sh} and x_{sl}, and weak solution concentrations, x_{wh} and x_{wl}, at different pressure levels, in the high and low pressure loops, respectively. x_{sh} and x_{sl} could have the same value if the generator is heated uniformly, and they can be straightforward determined since they are at the intersection point of P_l and $T_{g,e}$; whereas x_{wh} and x_{wl} are unnecessarily the same but depend on the recirculation flow ratios of both high pressure loop (FR_h) and low pressure loop (FR_l), and another key parameter – the flow fraction (f_r) of the refrigerant in high pressure loop to the total refrigerant flow. All the other unknown parameters can be solved through the following steps with an iterated calculation:

1. The value of f_r is hypothesised at 0.5 (or any other value between 0 and 1), then the flow rates of the two refrigerant streams, $\dot{m}_{rl}$ and $\dot{m}_{rh}$, are obtained as $\dot{m}_r$ is already given;

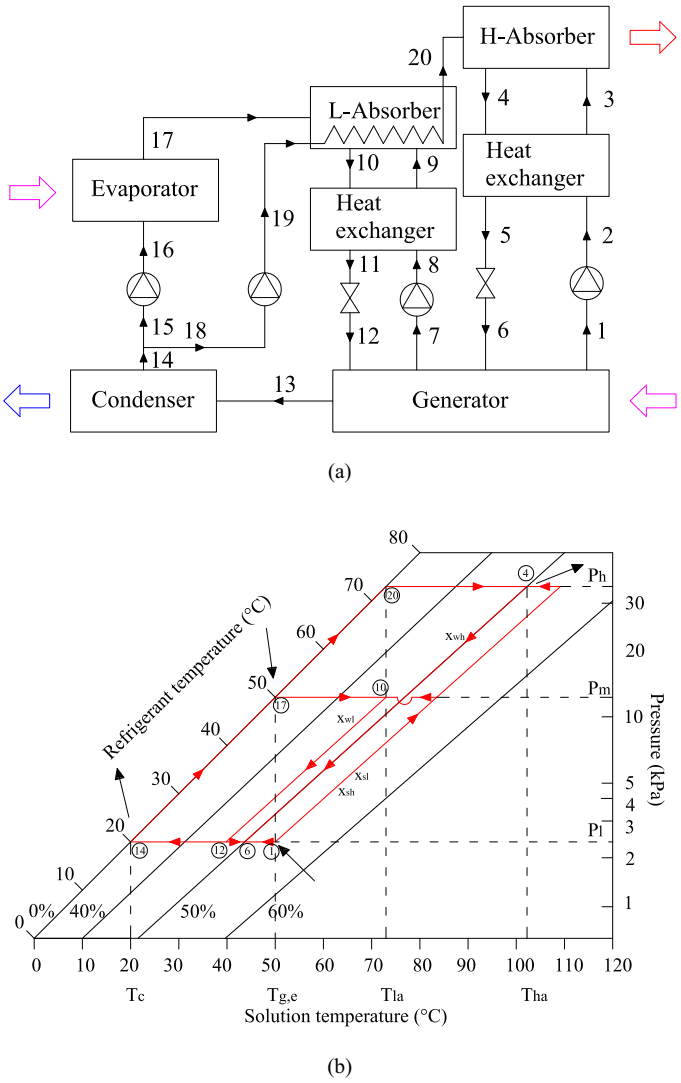

Fig. 2. DAHT-1. (a) Schematic diagram; (b) P–T–x diagram.

2. The x_{wl}, x_{wh}, $\dot{m}_{wl}$, $\dot{m}_{wh}$, $\dot{m}_{sl}$ and $\dot{m}_{sh}$ are obtained based on the given FR_l and FR_h, the already known x_{sl}, x_{sh} and $\dot{m}_{rl}$, $\dot{m}_{rh}$ with the aid of mass balance equations in both L-Absorber and H-Absorber (Eqs. (2) to (4));
3. The absorption temperature in L-Absorber ($T_{la} = T_{10}$) can be determined from Fig. 2(b) as it is at the intersection point of P_m and x_{wl};
4. The high pressure loop of the refrigeration is heated by L-Absorber (stream 19–20) and is ideally assumed to achieve the same temperature of absorption ($T_{20} = T_{la}$), then the saturation pressure of refrigerant at T_{la} is considered as the high pressure P_h in H-Absorber, as shown in Fig. 2(b);
5. Therefore, the absorption temperature in H-Absorber ($T_{ha} = T_4$) can be decided by P_h and x_{wh};
6. The Eqs. (12) and (13) are used to calculate the absorption heat released by L-Absorber ($Q_{L\text{-Absorption}}$) and the evaporation heat required by the refrigerant evaporation for H-Absorber ($Q_{H\text{-Evaporation}}$), respectively, and these two should have the same value if luckily the hypothetical f_r value is equal to the correct f_r value. If not, a new f_r should be re-hypothesised by considering the gap between $Q_{L\text{-Absorption}}$ and $Q_{H\text{-Evaporation}}$ and steps (2) to (6) should be repeated to calculate new $Q_{L\text{-Absorption}}$ and $Q_{H\text{-Evaporation}}$. The iteration will

Please cite this article in press as: Zhiwei Ma, Huashan Bao, Anthony Paul Roskilly, Performance analysis of ultralow grade waste heat upgrade using absorption heat transformer, Applied Thermal Engineering (2016), doi: 10.1016/j.applthermaleng.2016.02.002

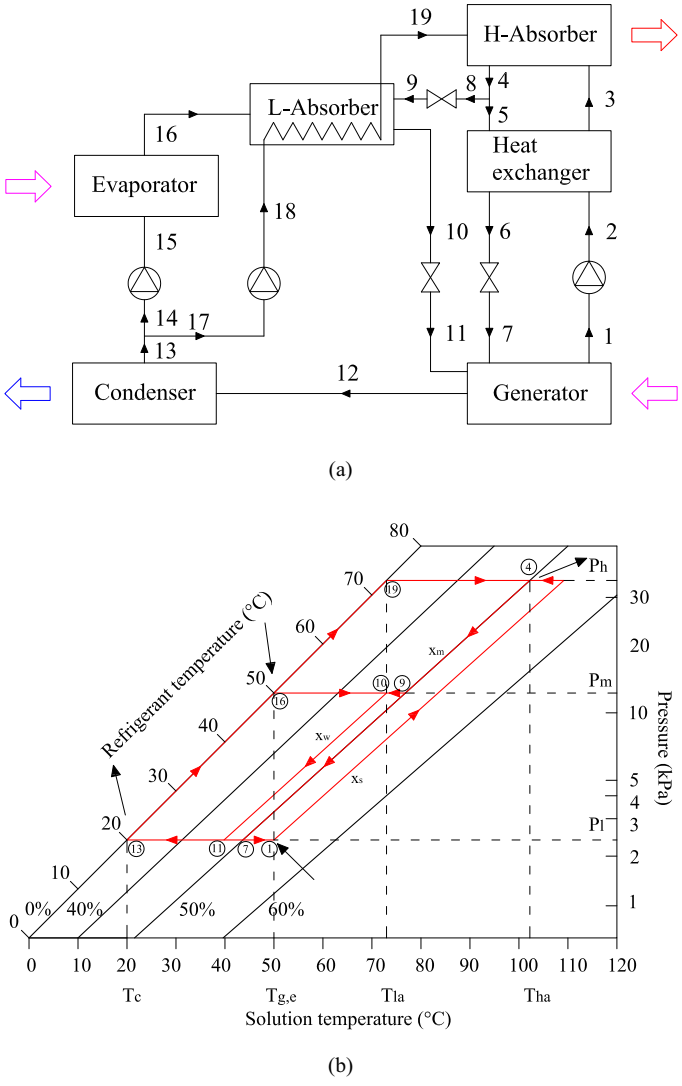

Fig. 3. DAHT-2. (a) Schematic diagram; (b) P–T–x diagram.

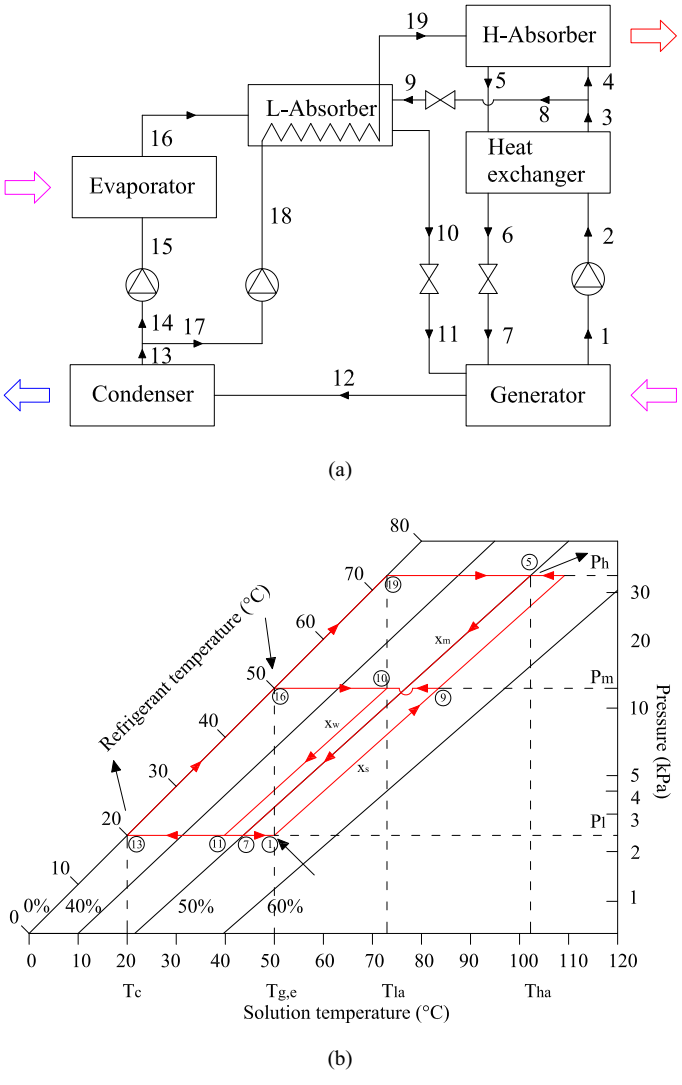

Fig. 4. DAHT-3. (a) Schematic diagram; (b) P–T–x diagram.

stop when reaching the convergence as $Q_{\text{L-Absorption}}$ equal to $Q_{\text{H-Evaporation}}$.

$$Q_{\text{L-Absorption}} = \dot{m}_{17}h_{17} + \dot{m}_9 h_9 - \dot{m}_{10}h_{10} \tag{12}$$

$$Q_{\text{H-Evaporation}} = \dot{m}_{20}(h_{20} - h_{19}) \tag{13}$$

2.3. DAHT-2 and DAHT-3

DAHT-2 and DAHT-3 have similar configuration, as presented in Figs. 3(a) and 4(a). Three different solutions are involved in DAHT-2 and DAHT-3, named as strong solution (x_s), medium solution (x_m), and weak solution (x_w). DAHT-2 and DAHT-3 have only one more L-Absorber compared to the SAHT. In DAHT-2, as shown in Fig. 3(a), part of the medium solution from the H-Absorber feeds into the L-Absorber (stream 4-8-9) as the absorbent that absorbs the refrigerant vapour to form the weak solution; meanwhile the rest part of the medium solution from the H-Absorber flows back to the generator (stream 4-5-6-7). In DAHT-3, as shown in Fig. 4(a), the absorbent in the L-Absorber derives from the part of the strong solution leaving the generator (stream 3-8-9). Their corresponding P–T–x diagrams are shown in Figs. 3(b) and 4(b) respectively.

For both DAHT-2 and DAHT-3, P_l, P_m and x_s are determined by condensation temperature T_c and waste heat temperature $T_{g,e}$. Aside from all the variables defined in the SAHT cycle, the flow fraction, f_w, of the weak solution leaving the L-Absorber to the total flow rate of solution flowing back to the generator is another indispensable parameter to solve all the puzzles of DAHT-2 and DAHT-3 cycles. The flow rates of the strong solution, the medium solution and the weak solution can be calculated with the given FR, f_w and $\dot{m}_r$. Similarly to the calculation steps for DAHT-1, the value of the flow fraction f_r is firstly set to be 0.5 to initiate the iterated calculation in this work until the final convergence is reached. The flow rates of two streams of the refrigerant are calculated firstly based on the hypothetical f_r, then the concentrations of the medium and the weak solutions can be determined by using the mass balance equations in the H-Absorber and the generator, respectively. The absorption temperature in the L-Absorber, T_{la}, is determined by the intersection point of P_m and x_w; while the high pressure P_h is the saturation pressure of refrigerant at T_{la} and the absorber temperature in the H-Absorber, T_{ha}, is at the intersection point of P_h and x_m in Figs. 3(b) and 4(b). The value of f_r must be iterated until achieving the thermal balance in L-Absorber using the similar equation as Eqs. (12) and (13).

Please cite this article in press as: Zhiwei Ma, Huashan Bao, Anthony Paul Roskilly, Performance analysis of ultralow grade waste heat upgrade using absorption heat transformer, Applied Thermal Engineering (2016), doi: 10.1016/j.applthermaleng.2016.02.002

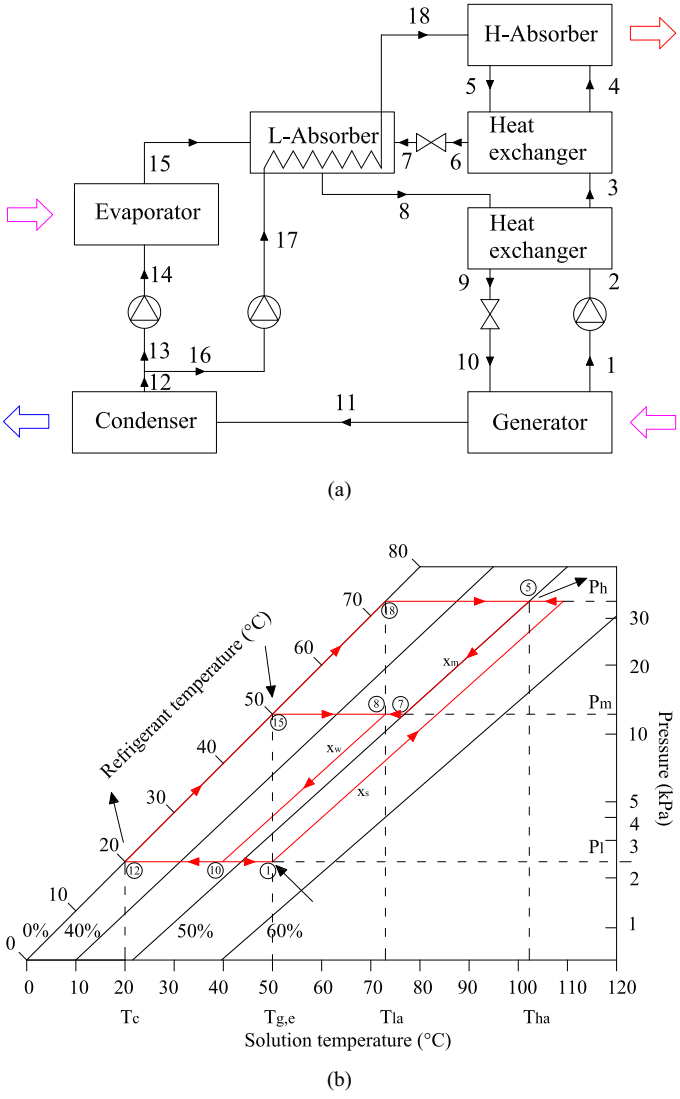

Fig. 5. DAHT-4. (a) Schematic diagram; (b) P–T–x diagram.

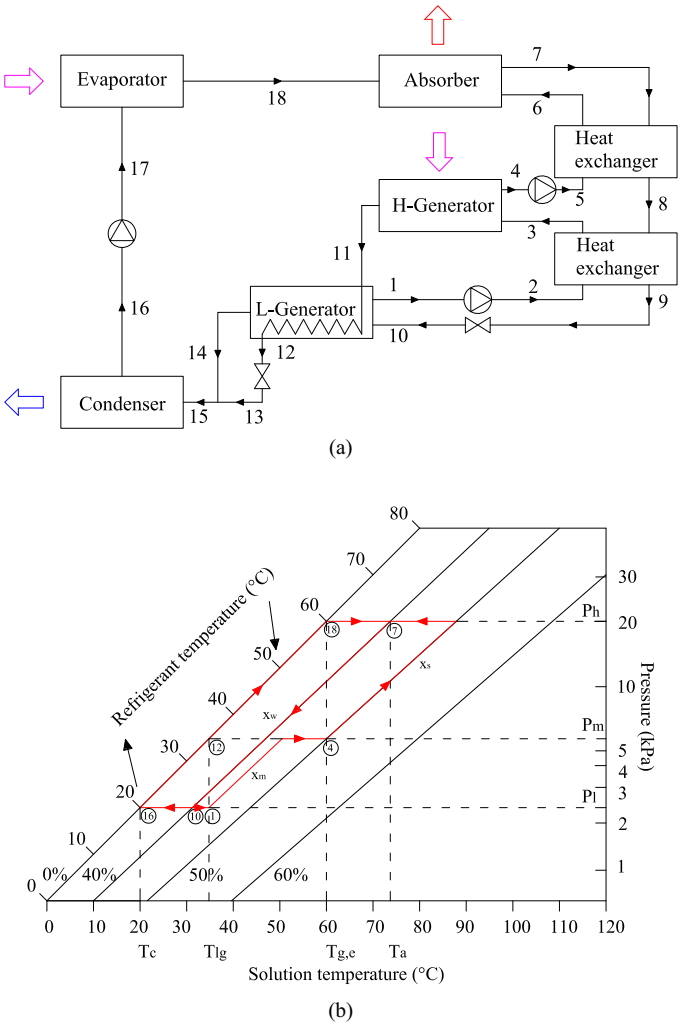

Fig. 6. DeAHT. (a) Schematic diagram; (b) P–T–x diagram.

2.4. DAHT-4

DAHT-4 shown in Fig. 5(a) has simpler configuration in terms of flow control: no splitting of solution is involved as all the medium solution coming from the H-Absorber feeds into the L-Absorber to conduct absorption (stream 5-6-7), afterwards it becomes weak solution and flows back to the generator (stream 8-9-10).

The low pressure (P_l) and medium pressure (P_m) are determined by the equilibrium state of refrigerant at T_c and $T_{g,e}$, then x_s and x_w, $\dot{m}_s$ and $\dot{m}_w$ are calculated based on P_l, $T_{g,e}$, predefined FR, $\dot{m}_r$ and the mass balance in generator. Thereafter, the absorption temperature in L-Absorber (T_{la}) can be determined by P_m and x_w as shown in Fig. 5(b). The high absorption pressure P_h is then the saturation pressure of refrigerant at T_{la}. With an initial hypothetical value of f_r, the mass balance equation in H-Absorber is used to calculate x_m and $\dot{m}_m$, thus the high absorption temperature T_{ha} becomes known. Eventually, the entire cycle can be established by identifying the f_r through the iteration to achieve the thermal balance in L-Absorber.

2.5. DeAHT

The double effect AHT (DeAHT) shown in Fig. 6(a) has two generators at two different pressure levels instead of two absorbers in DAHTs. The waste heat is used to heat the generator at the high pressure (H-Generator) and herein generate the refrigerant vapour out from the medium solution; then the condensation heat of the vapour is used to heat up the weak solution (stream 11–12) in the low pressure L-Generator to generate low pressure refrigerant vapour. Afterwards, the cooled down refrigerant passes through a throttle device (stream 12–13) and then converges with the refrigerant vapour from L-Generator within the condenser (stream 13,14–15). The weak solution from the only absorber directly heads to the L-Generator (stream 7-8-9-10) that discharges enriched solution (the medium solution) to the H-Generator (stream 1-2-3), while the H-Generator drains the strong solution to the absorber (stream 4-5-6).

The DeAHT cycle cannot operate if the so-called strong solution is not strong enough, neither the waste heat temperature is not high enough. The present study has used a given strong solution concentration, x_s, as a start to solve all the other solution and refrigerant states. The pressures, P_l, P_m and P_h, can be determined by the saturated state of the refrigerant at T_c, the saturated state of the strong solution at $T_{g,e}$ and the saturated state of the refrigerant at $T_{g,e}$, respectively, as shown in Fig. 6(b). The temperature in the L-Generator, T_{lg}, should be the condensing temperature of the refrigerant vapour from the H-Generator, which is the refrigerant saturation temperature at pressure P_m. Thereafter, the concentration of the medium solution, x_m, is the saturation solution

Please cite this article in press as: Zhiwei Ma, Huashan Bao, Anthony Paul Roskilly, Performance analysis of ultralow grade waste heat upgrade using absorption heat transformer, Applied Thermal Engineering (2016), doi: 10.1016/j.applthermaleng.2016.02.002

Table 1
Input parameters for the calculations.

	SAHT	DAHT-1	DAHT-2	DAHT-3	DAHT-4	DeAHT
$\dot{m}_r$ (kg/s)	0.005	0.005	0.005	0.005	0.005	0.005
T_c (°C)	10–30	20	20	20	20	10
FR (-)	2–20	FR_l: 1–10 FR_h: 1–10	2–20	2–20	2–20	-
UA (W/K)	50–450	2*75	150	150	2*75	2*75
f_w (-)	–	–	0.1–0.7	0.1–0.7	–	–
x_s (-)	–	–	–	–	–	0.48–0.6

concentration at P_l and T_{lg}. Different from aforementioned DAHTs, the recirculation flow ratio, *FR* (here is the mass flow rate ratio of the strong solution to refrigerant flowing into the absorber), should be then iteratively approached to satisfy the thermal balance in the L-Generator by the following steps: with a given value of $\dot{m}_r$ and an initially assumed *FR*, the strong and weak solution flow rates in the absorber can be calculated; then the weak solution concentration x_w is determined by the mass balance in the absorber; a new *FR* can be attained by solving the thermal balance in L-Generator; with the precondition of $x_w < x_m$ (x_w and x_m are determined independently), the *FR* value is adjusted and iterated until acquiring a correct *FR* meeting all the conditions; thereafter all the other states can be worked out.

2.6. Input parameters and optimisation process

The input parameters for all the calculations for different AHTs studied in this work are presented in Table 1. The mass flow rate of refrigerant, $\dot{m}_r$, is the essential variable for the full set of calculation on system performance, which was assumed to be 0.005 kg/s in this work as suggested in reference [36] for a 10 kW level absorption refrigeration system. It was found that the temperature lift is insensitive to the changes of $\dot{m}_r$ value; and the impact of the varying $\dot{m}_r$ on system *COP* and *COPe* would be offset if the heat transfer parameter *UA* of the heat-recovery heat exchanger increases or reduces at the same ratio as the $\dot{m}_r$ does because of the proportional changes of the involved heat in each component. Reference [36] also suggested a typical design value of recirculation flow ratio, *FR*, as 10.84, and used a *UA* value of the heat-recovery heat exchanger as 132 W/K for one of the presented examples. Hence, the *UA* analysed in this work ranges from 50 W/K to 450 W/K, while the *FR* was set in the range of 2–20 to cover the full potential region of system operation.

The SAHT system performance was fully evaluated with each input parameter varying in a given range presented in Table 1 so that the most dominant factor for AHT systems could be identified. Thereafter, the influence of this factor on DAHTs and DeAHT were further discussed under the condition of 40~60 °C heat source. The relation of the energy efficiency and upgraded temperature were depicted for each heat source temperature to illustrate the influence of the varying parameters and to determine the optimal operation conditions.

3. Results and discussions

The calculation method has been validated with experimental results of SAHT reported in literature [14], as the calculated performance in this work and experimental results are compared in Fig. 7(a). The experiment was conducted under the conditions of T_g = 76.5~78.5 °C, T_e = 53.0~59.8 °C and T_c = 35.8~37.5 °C; COP_{int} was defined as the internal *COP*, of which the heat was calculated based on the enthalpy change of the solution and refrigerant, while the external *COP*, COP_{ext}, was calculated based on the heat released or absorbed by the external heat transfer fluids. The present calculation used the same operational conditions as the experiment, and the calculated *COP* shows good agreement with the experimental COP_{int} as can be seen in Fig. 7(a) when the *FR* is about 5.4–5.8.

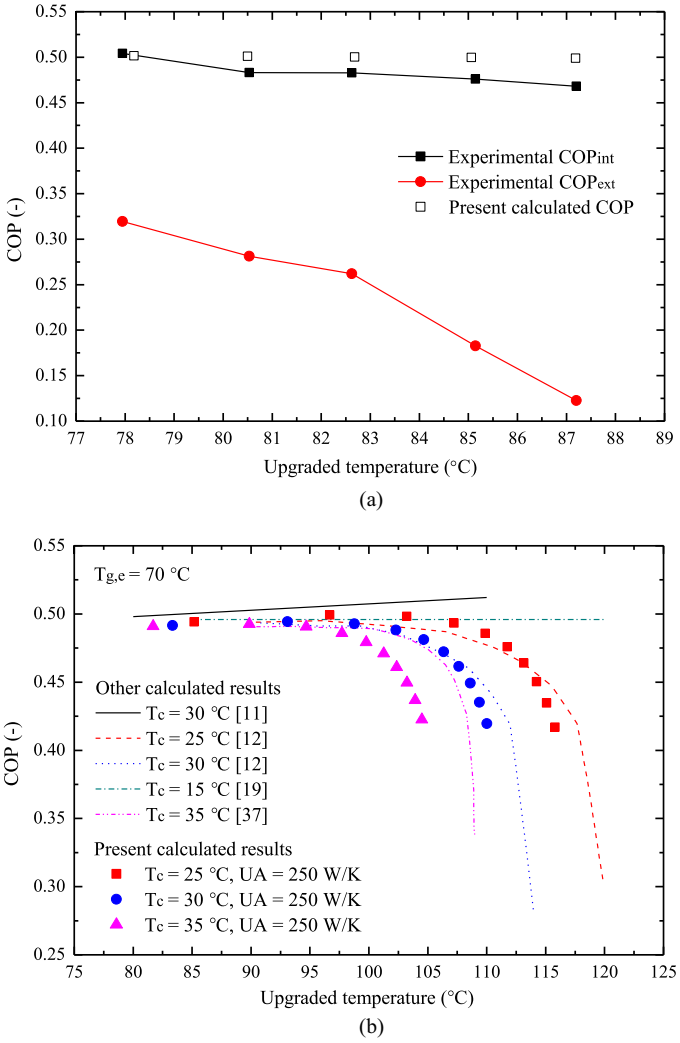

Fig. 7. (a) Validation of the calculated method by experimental results of SAHT [14] with T_g = 76.5–78.5 °C, T_e = 53.0–59.8 °C and T_c = 35.8–37.5 °C; (b) comparison between present calculated *COP* with others [11,12,19,37], $T_{g,e}$ = 70 °C.

The *COP* value calculated in this work is also compared with other analysis results reported previously in references 11, 12, 19, and 37, as shown in Fig. 7(b), while the generation temperature and the evaporation temperature at 70 °C were used in all compared cases. Kurem and Horuz [11] and Yin et al. [19] obtained almost constant *COP* of around 0.495~0.515 even when the temperature lift was as high as 40~50 °C. The *COP* results in this work show the similar variation profile against the upgraded heat temperature to those reported by Rivera et al. [12] and Zhang and Hu [37], and the *COP* values are almost the same with those in reference 12 when the *UA* value is assumed as 250 W/K. The *COP* values have no prominent change if the upgraded heat is at relatively low temperature, as shown in Fig. 7(b) from 80 °C to 95 °C, or to 100 °C, or to 105 °C, depending on different condensing temperature. Once exceeding these ranges, the *COP* values drop steeply afterwards.

3.1. SAHT

The performance of SAHT is dominated by several parameters, including waste heat temperature $T_{g,e}$, condensation temperature

Please cite this article in press as: Zhiwei Ma, Huashan Bao, Anthony Paul Roskilly, Performance analysis of ultralow grade waste heat upgrade using absorption heat transformer, Applied Thermal Engineering (2016), doi: 10.1016/j.applthermaleng.2016.02.002

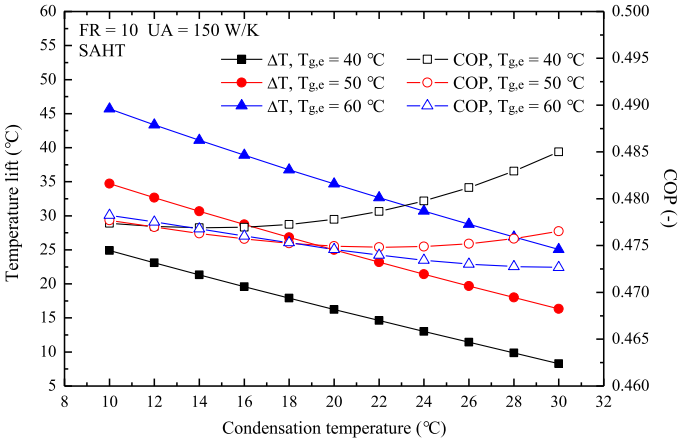

Fig. 8. Temperature lift and *COP* with varying condensation temperature in SAHT, while *FR* = 10 and *UA* = 150 W/K.

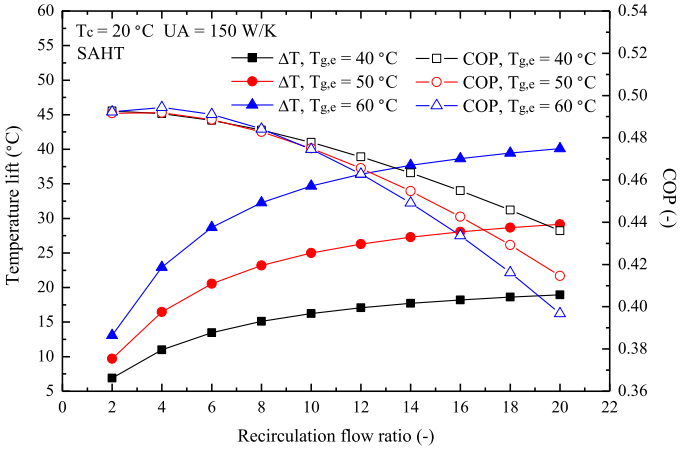

Fig. 9. Temperature lift and *COP* with varying recirculation flow ratio in SAHT, while T_c = 20 °C and *UA* = 150 W/K.

T_c, recirculation flow ratio *FR*, and the performance of heat exchanger *UA*.

Fig. 8 shows the calculated temperature lift and *COP* against the varying condensation temperature T_c from 10 °C to 30 °C at the condition of *FR* = 10 and *UA* = 150 W/K. The figure shows a temperature lift of 8.3~24.9 °C with 40 °C heat source, 16.3~34.7 °C with 50 °C heat source and 25.1~45.7 °C with 60 °C heat source. The lower condensation temperature is, the higher temperature lift can be by using a fixed waste heat temperature, which can be explained by that a lower condensation temperature allows a lower pressure in the condenser and the generator so that the waste heat can deal with stronger solution in generator, resulting in the relatively stronger weak solution in the absorber, and then the absorption temperature is higher that indicates a larger temperature lift. Unlike the temperature lift, *COP* value changes in a narrow range of 0.47~0.485 and is hardly affected by the condensation temperature, e.g. the fluctuation of *COP* value is basically less than 0.01 when the condensation temperature ranges from 10 to 30 °C regardless of waste heat temperature, which can be explained by the following reasons: (1) the flow rates of strong and weak solutions remain unchanged due to the same *FR* and $\dot{m}_r$; (2) the concentration difference between strong and weak solutions hardly change due to the same *FR* that ensures a constant value of the ratio of x_s to x_w; (3) therefore both the input heat to the generator and output heat from the absorber change little and have the same changing tendency; (4) the input energy to the evaporator changes little, hence the calculated *COP* by Eq. (10) is not sensitive to the varying condensation temperature.

The most direct and crucial parameter that simultaneously affects both the temperature lift and *COP* is the recirculation flow ratio, *FR*, as illustrated in Fig. 9. A higher *FR* suggests a smaller concentration difference between the strong solution and the weak solution as can be derived from Eqs. (2) to (4), thus the weak solution concentration is relatively higher given that the strong solution concentration is fixed. Higher concentration of weak solution indicates higher absorption temperature (T_a) in the absorber at the same pressure (P_h), i.e. larger temperature lift. Therefore, as *FR* increases in the range of 2–20 while the condensation temperature and heat exchanger performance are fixed at 20 °C and 150 W/K, the temperature lifts of the waste heat at 40 °C, 50 °C and 60 °C display increasing curves within the range of 6.9~18.9 °C, 9.7~29.2 °C and 13.1~40.1 °C, respectively. Moreover, the decreasing concentration difference between strong and weak solution causes the reduction of the heat input required by the generator and heat output from the absorber, though flow rates of both solutions increase with increasing *FR*; nevertheless, the heat input to the evaporator remains constant with increasing *FR* due to the constant refrigerant flow rate and evaporation temperature. Hence the *COP* calculated by Eq. (10) reduces as the *FR* value increases, e.g. the *COP* is around 0.397 when *FR* is at 20 and the waste heat is at 60 °C, which is about 20% lower than the maximum *COP* value (0.494).

The heat exchanger located between generator and absorber is deployed to enhance the system efficiency. The performance parameter of the heat exchanger, *UA*, has no impact on the temperature lift but is influential on the *COP*. A higher *UA* leads to better heat recovery, i.e. more heat input to the generator and heat output from the absorber; with constant heat input to the evaporation, the *COP* shows upward trend with the increasing *UA* as shown in Fig. 10, e.g. the *COP* of using 60 °C waste heat increases from about 0.452 to 0.492 as the *UA* increases from 50 W/K to 450 W/K when *FR* is at 10 and the condensation temperature is at 20 °C.

Fig. 11 shows the exergy coefficient, *COPe*, of SAHT against the upgraded temperature under the conditions of T_c = 20 °C and *UA* = 150 W/K. The values of *FR* are denoted as dash lines in the figure. As can be seen from the calculation equation, Eq. (11), *COPe* reflects both *COP* and temperature lift. Although the *COP* decreases as increasing *FR*, the *COPe* surges as *FR* increases until 10 due to the increasing output heat temperature, followed by reaching its vertex and subsequently declining. Based on the value of *COPe*, the optimal

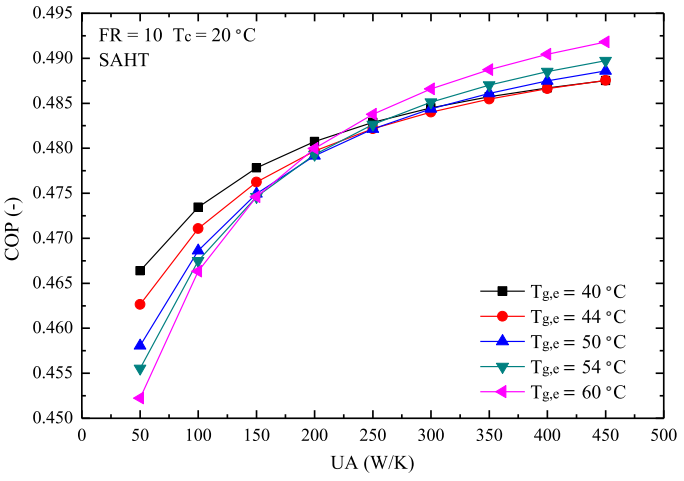

Fig. 10. *COP* with varying heat exchanger performance in SAHT, while *FR* = 10 and T_c = 20 °C.

Please cite this article in press as: Zhiwei Ma, Huashan Bao, Anthony Paul Roskilly, Performance analysis of ultralow grade waste heat upgrade using absorption heat transformer, Applied Thermal Engineering (2016), doi: 10.1016/j.applthermaleng.2016.02.002

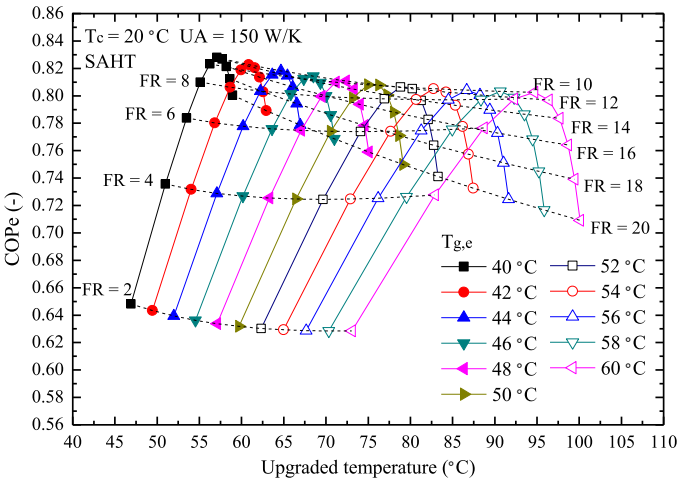

Fig. 11. *COPe* vs. upgraded temperature with varying waste heat temperature and recirculation flow ratio in SAHT, while $T_c = 20$ °C and $UA = 150$ W/K.

FR locates between 10 and 12 for SAHT, where the *COPe* reaches its maximum value of 0.803~0.828 while the corresponding *COP* is 0.471~0.475 and the temperature lift is 17.1~34.7 °C depending on different waste heat temperature. Of course, one can pursue higher temperature lift by using larger *FR* if the lower *COP* is acceptable, vice versa.

3.2. DAHTs

The performance of the four DAHTs are compared in terms of temperature lift, *COP* and *COPe* as shown in Fig. 12(a) and (b), which present the calculation results of *COP* and *COPe* against the upgraded temperature respectively under the condition of $T_c = 20$ °C and $UA = 150$ W/K. The best performance in terms of the highest *COPe* of DAHT-2 and DAHT-3 are shown in Fig. 12 with the value of f_w varying in the range of 0.1~0.7. For all the studied cases, the optimal f_w was found at around 0.5.

As shown in the figure, the DAHT cycles could produce a temperature lift of 14.1~41.2 °C by 40 °C waste heat, 20.0~62.9 °C by 50 °C waste heat and 27.1~86.1 °C by 60 °C waste heat, which are almost twice as large as that produced by SAHT. However, the larger temperature lift implies the compromised system efficiency, e.g. the maximum *COP* value is only about 0.322, whereas the minimum one could be as low as less than 0.01 while the temperature lift reaches the maximum potential. Sharing the similar varying tendency with that of SAHT, the *COPe* of different DAHTs in Fig. 12(b) has the maximum values from 0.614 to 0.708 depending on different waste heat temperature, which is lower than that of SAHT. Through the comparison shown in the figures, DAHT-4 exhibits the highest values of both *COP* and *COPe* among these four different DAHTs, while the DAHT-1 and DAHT-3 have slightly lower efficiencies and the DAHT-2 has the lowest. Additionally, the simplest configuration and solution flow control of the DAHT-4 further strengthens its competitive advantage over the other three.

In Fig. 13, the temperature lift and *COP* values of the best DAHT, DAHT-4, are plotted against recirculation flow ratio in the range of 2~20. The curves shown in the figure are similar to those shown in Fig. 9 for SAHT. The increase of *FR* leads to gradually increasing temperature lift but drastic *COP* reduction, which can be explained by the same reason as that of SAHT. The maximum *COP* value is around 0.322 regardless of the waste heat temperature. Comparing to SAHT, the impact of *FR* on the *COP* is amplified in DAHTs. Since the increase of *FR* in DAHTs implicates even smaller differences between the concentrations of strong and the medium solutions in the H-Absorber, the output heat from the absorber reduces more steeply than that in SAHT, which sometimes can even drop to null and leads to a *COP* near 0 as shown in the Fig. 13.

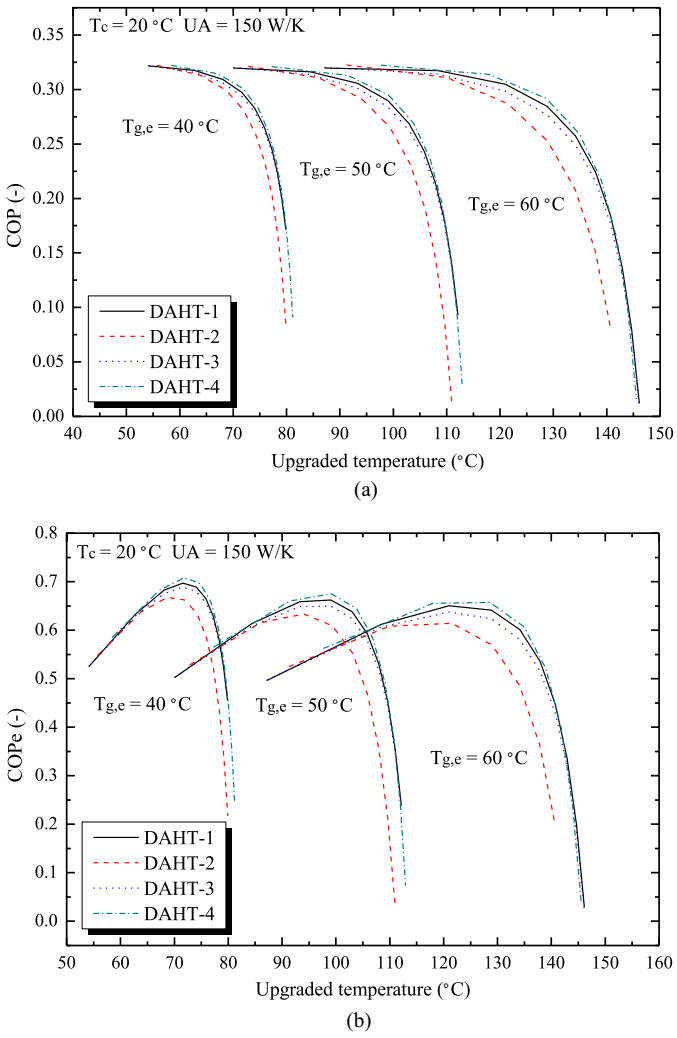

Fig. 12. (a) *COP* and (b) *COPe* vs. upgraded temperature with 40 °C, 50 °C and 60 °C waste heat in DAHTs, while $T_c = 20$ °C and $UA = 150$ W/K.

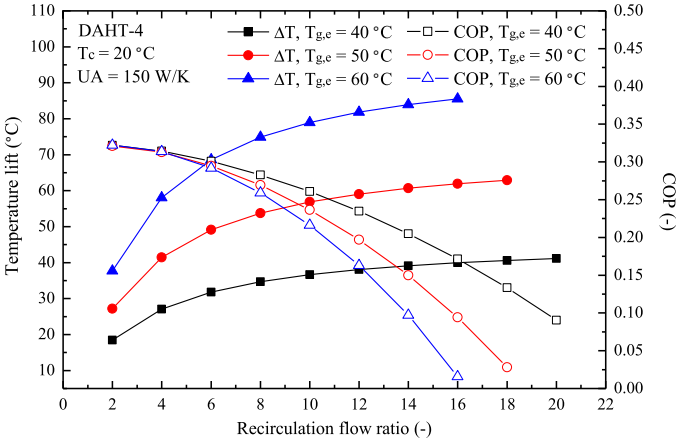

Fig. 13. Temperature lift and *COP* with varying recirculation flow ratio in DAHT-4, while $T_c = 20$ °C and $UA = 150$ W/K.

Please cite this article in press as: Zhiwei Ma, Huashan Bao, Anthony Paul Roskilly, Performance analysis of ultralow grade waste heat upgrade using absorption heat transformer, Applied Thermal Engineering (2016), doi: 10.1016/j.applthermaleng.2016.02.002

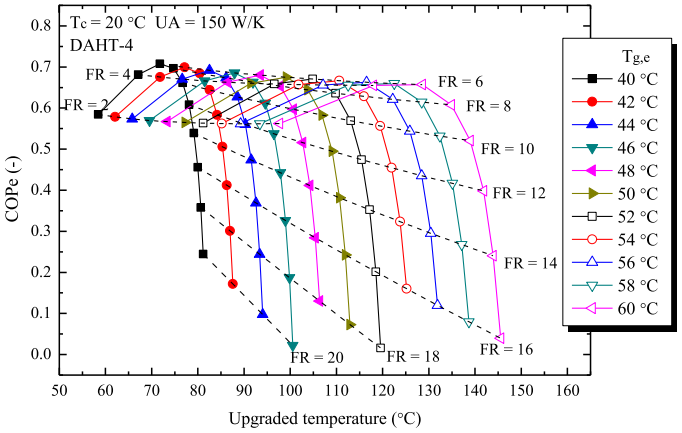

Fig. 14. *COPe* vs. upgraded temperature with varying waste heat temperature and recirculation flow ratio in DAHT-4, while $T_c = 20$ °C and $UA = 150$ W/K.

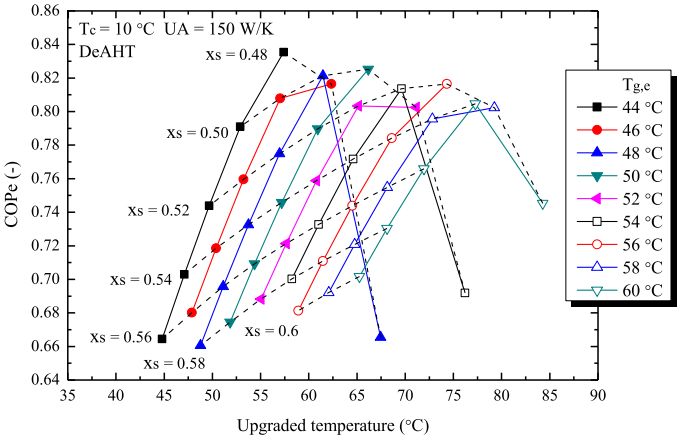

Fig. 16. *COPe* vs. upgraded temperature with varying waste heat temperature and strong solution concentration in DeAHT, while $T_c = 10$ °C and $UA = 150$ W/K.

Fig. 14 shows the *COPe* of DAHT-4 against the upgraded temperature. *COPe* has the peak value between 0.657 and 0.708 with the optimal *FR* at the value of 6 for all studied waste heat temperature, where the *COP* is around 0.292~0.301 and the temperature lift ranges from 31.8 to 68.6 °C.

3.3. DeAHT

As foregoing process description in Section 2.5, the operational condition in DeAHT is relatively demanding than other cycles studied in this work. It requires both the strong solution concentration and waste heat source temperature to be high enough to achieve the heat balance in the L-Generator and ensure the cycle implementation. In this work, 10 °C condensation temperature and 150 W/K heat transfer performance are applied to the calculation in order to maximise the usage of waste heat in the temperature range. In this instance, the threshold of the strong solution concentration and the waste heat temperature is 0.48 and 44 °C, respectively.

Fig. 15 shows the temperature lift and the *COP* of DeAHT against strong solution concentration. Due to the double effect generation, the maximum *COP* value of the DeAHT is about 0.65, which is about 35% and 100% higher than those of SAHT and DAHTs respectively; however, the corresponding temperature lift is much lower than those of SAHT and DAHTs. The DeAHT can only achieve a temperature lift of 0.8~13.4 °C with 44 °C waste heat, 1.8~16.2 °C with 50 °C waste heat and 5.3~24.3 °C with 60 °C waste heat. As an input parameter, higher strong solution concentration causes a lower pressure in the L-Absorber as can be seen in Fig. 6(b), thus relatively lower medium and weak solution concentrations are expected that results in a lower output temperature in absorber and then smaller temperature lift. With higher strong solution concentration, the larger concentration difference among the involved three solutions implies a lower value of *FR*, e.g. *FR* decreases from about 12.4 to 0.8 when x_s increases from 0.52 to 0.6 for 60 °C waste heat. However, the reducing *FR* does not lead to an increasing *COP* of DeAHT as SAHT and DAHT do. The reason of this contradictory result could be possibly explained as DeAHT requires quite large concentration difference when x_s is high, e.g. $x_w = 0.27$ and $x_m = 0.38$ when $x_s = 0.6$, then the non-linear variation of the LiBr solution enthalpy against solution concentration causes the non-linear changes of input/output heat and generally increasing system *COP* with x_s.

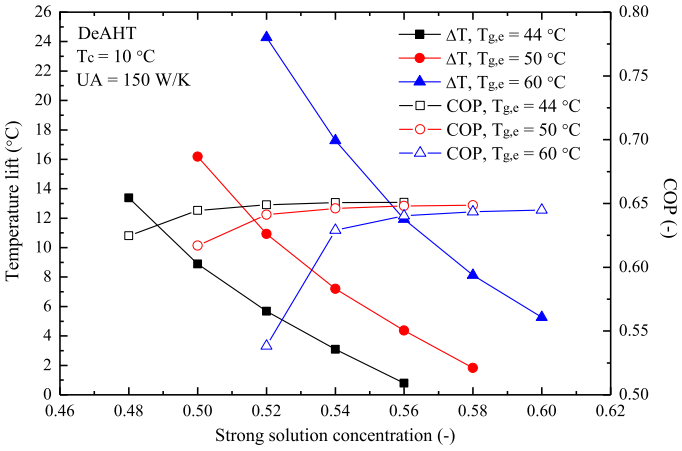

Fig. 15. Temperature lift and *COP* with varying strong solution concentration in DeAHT, while $T_c = 10$ °C and $UA = 150$ W/K.

The *COPe* of DeAHT shown in Fig. 16 is in the range of 0.664~0.835 and is in function of waste heat temperature, upgraded temperature and strong solution concentration. The graphic information suggests each optimal strong solution concentration to obtain maximum *COPe* value when the waste heat is at 48 °C, 52 °C, 54 °C and 60 °C, respectively. The DeAHT with waste heat source at other temperatures in Fig. 16 has untapped potential under the studied condition due to the aforementioned demanding operational requirement.

3.4. Comparison of AHTs

The performance comparison of SAHT, the best DAHT, i.e. DAHT-4, and DeAHT is presented in Fig. 17(a) to (c) in terms of the temperature lift, *COP* and *COPe*, respectively, while Table 2 lists the optimal working performances of these AHTs based on the maximum *COPe* values.

It is noticeable that the SAHT performance is in between the other two systems, with medium temperature lift as well as medium efficiencies. The DAHT-4 has the largest temperature lift, but with the lowest *COP* and *COPe*. The DeAHT exhibits the best heat transformation *COP* with the lowest temperature lift for the ultralow grade waste heat utilisation studied in this work. It should be noticed that the *COPe* of DeAHT is not better than that of SAHT. Because of the demanding operational conditions, relatively lower temperature lift, modest *COPe* and relatively complex configuration, the DeAHT is not recommended for heat transformation of 40~60 °C ultralow grade heat despite of its highest *COP*.

Please cite this article in press as: Zhiwei Ma, Huashan Bao, Anthony Paul Roskilly, Performance analysis of ultralow grade waste heat upgrade using absorption heat transformer, Applied Thermal Engineering (2016), doi: 10.1016/j.applthermaleng.2016.02.002

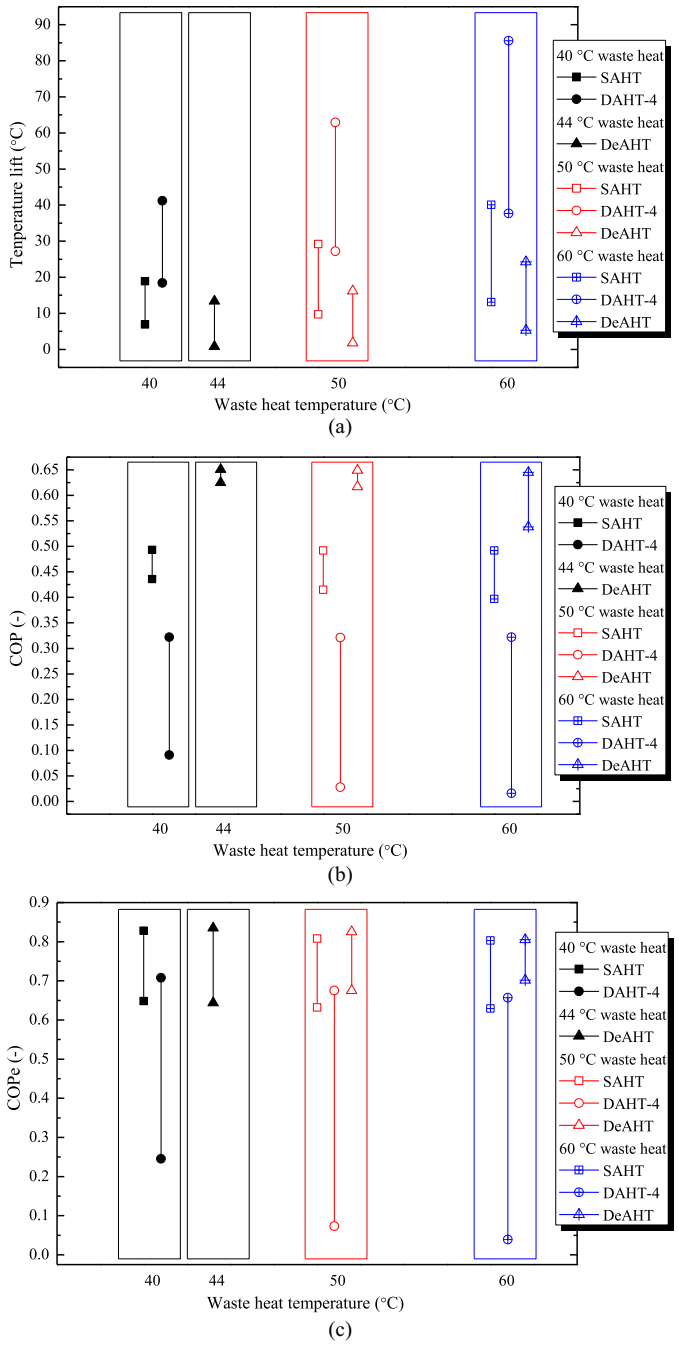

Fig. 17. Performance comparison of SAHT, DAHT-4 and DeAHT. (a) Temperature lift; (b) *COP*; and (c) *COPe*.

4. Conclusions

The present paper investigated the absorption heat transformers to upgrade the ultralow grade waste heat in the temperature range from 40 to 60 °C. The performance of a single stage, four double stage and a double effect absorption heat transformers were numerically analysed and compared while the analytical methods have been validated with experimental data from other studies and also been constracted with other numerical approaches. The conclusions are summarised as follows.

1. The condensation temperature T_c had significant effect on temperature lift but hardly influenced the system efficiency. The recirculation flow ratio, *FR*, was found to be the most crucial factor for the AHTs performance. The temperature lift increased while *COP* decreased with the increasing *FR* value; there was an optimal value of *FR* to achieve maximum *COPe*, which reflected the temperature lift and the *COP* simultaneously.
2. SAHT yielded a medium temperature lift with medium system efficiency. The optimal value of *FR* was in the range of 10~12, depending on different waste heat temperature, and that led to the maximum *COPe* of 0.803~0.828 with the *COP* value ranging from 0.466 to 0.475 and the temperature lift from 17.1 to 34.7 °C.
3. DAHTs sacrificed the system efficiency to achieve higher temperature lift; DAHT-4 was the best DAHT among those studied in this work, which had the optimal performance of the *COPe* at 0.657~0.708, the *COP* at 0.292~0.301 and the temperature lift at 31.8~68.6 °C when *FR* was at 6.
4. The DeAHT application was limited by the requirements of relatively high input temperature and high concentration of the strong solution. It achieved the highest system *COP* and *COPe* compared to the other cycles studied; however, its temperature lift was the lowest. Provided with its other limitations, the DeAHT was considered to be not suitable for the upgrading of ultralow temperature waste heat.

Acknowledgements

The authors gratefully acknowledge the support from the IAA project (Impact Acceleration Account) (EP/K503885/1) and IDRIST project (EP/M008088/1), funded by the Engineering and Physical Science Research Council of UK.

Nomenclature

COP	Coefficient of performance [-]
COPe	Exergy coefficient of performance [-]
FR	Recirculation flow ratio [-]
f	Flow fraction [-]
h	Enthalpy [J/kg]

Table 2
The optimal working performances of SAHT, DAHT-4 and DeAHT.

	SAHT			DAHT-4			DeAHT		
	40 °C	50 °C	60 °C	40 °C	50 °C	60 °C	44 °C	50 °C	60 °C
FR (-)	12	10	10	6	6	6	5.86	6.25	4.02
x_s	0.483	0.542	0.591	0.483	0.542	0.591	0.48	0.5	0.54
Temperature lift (°C)	17.1	25.0	34.7	31.8	49.1	68.6	13.4	16.2	17.3
COP (-)	0.471	0.475	0.475	0.301	0.295	0.292	0.625	0.617	0.629
COPe (-)	0.828	0.808	0.803	0.708	0.675	0.657	0.835	0.825	0.805

Please cite this article in press as: Zhiwei Ma, Huashan Bao, Anthony Paul Roskilly, Performance analysis of ultralow grade waste heat upgrade using absorption heat transformer, Applied Thermal Engineering (2016), doi: 10.1016/j.applthermaleng.2016.02.002

$\dot{m}$	Mass flow rate [kg/s]
Q	Heat [J]
T	Temperature [°C]
ΔT	Temperature lift [°C]
ΔT_{LMTD}	Logarithmic mean temperature difference [°C]
UA	Heat exchanger performance [W/K]
x	Solution concentration by weight [-]

Subscripts

a	Absorber
e	Evaporator
g	Generator
H, h	High pressure
HE	Heat exchanger
L, l	Low pressure
m	Medium solution
r	Refrigerant
s	Strong solution
w	Weak solution

References

[1] Department of Energy and Climate Change. Energy consumption in the UK. 2015.
[2] Element Energy Limited. The potential for recovering and using surplus heat from industrial, final report for DECC. 2014.
[3] F. Velez, J.J. Segovia, M.C. Martin, G. Antolin, F. Chejne, A. Quijano, A technical, economical and market review of organic Rankine cycles for the conversion of low grade heat for power generation, Renew. Sustain. Energy Rev. 16 (2012) 4175–4189.
[4] X. Zhang, M. He, Y. Zhang, A review of research on the Kalina cycle, Renew. Sustain. Energy Rev. 16 (2012) 5309–5318.
[5] X.Q. Zhai, M. Qu, Y. Li, R.Z. Wang, A review for research and new design options of solar absorption cooling systems, Renew. Sustain. Energy Rev. 15 (2011) 4416–4423.
[6] T.X. Li, R.Z. Wang, H. Li, Progress in the development of solid-gas sorption refrigeration thermodynamic cycle driven by low-grade thermal energy, Prog. Energ. Combust. Sci. 40 (2014) 1–58.
[7] H. Fang, J. Xia, K. Zhu, Y. Su, Y. Jiang, Industrial waste heat utilization for low temperature district heating, Energy Policy 62 (2013) 236–246.
[8] S. Brueckner, L. Miro, L.F. Cabeza, M. Pehnt, E. Laevemann, Methods to estimate the industrial waste heat potential of regions – a categorization and literature review, Renew. Sustain. Energy Rev. 38 (2014) 164–171.
[9] K. Parham, M. Khamooshi, D.B.K. Tematio, M. Yari, Absorption heat transformers – a comprehensive review, Renew. Sustain. Energy Rev. 34 (2014) 430–452.
[10] P. Donnellan, K. Cronin, E. Byrne, Recycling waste heat energy using vapour absorption heat transformers: a review, Renew. Sustain. Energy Rev. 42 (2015) 1290–1304.
[11] E. Kurem, I. Horuz, A comparison between ammonia-water and water-lithium bromide solutions in absorption heat transformers, Int. Commun. Heat Mass Transf. 28 (2001) 427–438.
[12] W. Rivera, R.J. Romero, M.J. Cardoso, J. Aguillon, R. Best, Theoretical and experimental comparison of the performance of a single-stage heat transformer operating with water/lithium bromide and water/Carrol™, Int. J. Energy Res. 26 (2002) 747–762.
[13] W. Rivera, J. Cerezo, Experimental study of the use of additives in the performance of a single-stage heat transformer operating with water–lithium bromide, Int. J. Energy Res. 29 (2005) 121–130.
[14] W. Rivera, H. Martinez, J. Cerezo, R.J. Romero, M.J. Cardoso, Exergy analysis of an experimental single-stage heat transformer operating with single water/lithium bromide and using additives (1-octanol and 2-ethyl-1-hexanol), Appl. Therm. Eng. 31 (2011) 3526–3532.
[15] R.M. Barragan, C.L. Herad, V.M. Arellano, R. Best, F.A. Holland, Experimental performance of the water / lithium chloride system in a heat transformer, Int. J. Energy Res. 19 (1995) 593–602.
[16] R.M. Barragan, C.L. Herad, V.M. Arellano, Experimental performance of the water/calcium chloride system in a heat transformer, Int. J. Energy Res. 20 (1996) 651–661.
[17] R.M. Barragan, V.M. Arellano, C.L. Herad, R. Best, F.A. Holland, Experimental performance of the water / magnesium chloride system in a heat transformer, Int. J. Energy Res. 21 (1997) 139–151.
[18] R.M. Barragan, V.M. Arellano, C.L. Herad, R. Best, Experimental performance of the ternary solutions in a heat transformer, Int. J. Energy Res. 22 (1998) 73–83.
[19] J. Yin, L. Shi, M.S. Zhu, L.Z. Han, Performance analysis of an absorption heat transformer with different working fluid combinations, Appl. Energy 67 (2000) 281–292.
[20] I. Horuz, B. Kurt, Absorption heat transformers and an industrial application, Renew. Energy 35 (2010) 2175–2181.
[21] K. Parham, M. Yari, U. Atikol, Alternative absorption heat transformer configurations integrated with water desalination system, Desalination 328 (2013) 74–82.
[22] W. Rivera, R. Best, J. Hernandez, C.L. Heard, F.A. Holland, Thermodynamic study of advanced absorption heat transformers – I. Single and two stage configurations with heat exchangers, Heat Recov. Syst. CHP 14 (1994) 173–183.
[23] W. Rivera, R. Best, J. Hernandez, C.L. Heard, F.A. Holland, Thermodynamic study of advanced absorption heat transformers – II. Double absorption configurations, Heat Recov. Syst. CHP 14 (1994) 185–193.
[24] R.J. Romero, S. Silva-Sotelo, J. Cerezo, First double stage heat transformer (Dsht) in Latin America, Chem. Eng. Trans. 19 (2010) 149–155.
[25] S.A. Fartaj, Comparison of energy, exergy, and entropy balance methods for analysis double-stage absorption heat transformer cycles, Int. J. Energy Res. 28 (2004) 1219–1230.
[26] J. Ji, M. Ishida, Behavior of a two-stage absorption heat transformer combining latent and sensible heat exchange modes, Appl. Energy 62 (1999) 267–281.
[27] H. Martinez, W. Rivera, Energy and exergy analysis of a double absorption heat transformer operating with water/lithium bromide, Int. J. Energy Res. 33 (2009) 662–674.
[28] R.M.B. Reyes, V.M.A. Gomez, A. Garcia-Gutierrez, Performance modelling of single and double absorption heat transformers, Curr. Appl. Phys. 10 (2010) S244–S248.
[29] Z. Zhao, F. Zhou, X. Zhang, S. Li, The thermodynamic performance of a new solution cycle in double absorption heat transformer using water/lithium bromide as the working fluids, Int. J. Refrig. 26 (2003) 315–320.
[30] I. Horuz, B. Kurt, Single stage and double absorption heat transformers in an industrial application, Int. J. Energy Res. 33 (2009) 787–798.
[31] C. Mostofizadeh, C. Kulick, Use of a new type of heat transformer in process industry, Appl. Therm. Eng. 18 (1998) 857–874.
[32] Z. Zhao, Y. Ma, J. Chen, Thermodynamic performance of a new type of double absorption heat transformer, Appl. Therm. Eng. 23 (2003) 2407–2414.
[33] Z. Zhao, X. Zhang, X. Ma, Thermodynamic performance of a double-effect absorption heat-transformer using TFE/E181 as the working fluid, Appl. Energy 82 (2005) 107–116.
[34] R. Gomri, Thermal seawater desalination: possibilities of using single effect and double effect absorption heat transformer systems, Desalination 235 (2010) 112–118.
[35] J. Pátek, J. Klomfar, A computationally effective formulation of the thermodynamic properties of LiBr-H_2O solution from 273 to 500 K over full composition range, Int. J. Refrig. 29 (2006) 566–578.
[36] K.E. Herold, R. Radermacher, S.A. Klein, Absorption Chillers and Heat Pumps. Chapter 6 Single-Effect Water/Lithium Bromide Systems, CRC Press, 1996.
[37] X. Zhang, D. Hu, Performance analysis of the single-stage absorption heat transformer using a new working pair composed of ionic liquid and water, Appl. Therm. Eng. 37 (2012) 129–135.

Please cite this article in press as: Zhiwei Ma, Huashan Bao, Anthony Paul Roskilly, Performance analysis of ultralow grade waste heat upgrade using absorption heat transformer, Applied Thermal Engineering (2016), doi: 10.1016/j.applthermaleng.2016.02.002